Proceedings of the ASME 2017 International Mechanical Engineering Congress & Exposition
IMECE 2017
November 3-9, 2017, Tampa, USA

IMECE2017-70805

AN ADAPTIVE TIME DOMAIN APPROACH TO CHARACTERIZE DISPERSIVE ELASTODYNAMIC MEDIA

Reza Abedi*
Mechanical, Aerospace & Biomedical Engineering
University of Tennessee Knoxville (UTK) /
Space Institute (UTSI)
Tullahoma, Tennessee, 37388

ABSTRACT

A time domain approach is presented to compute the transmission and reflection coefficients of a unit cell. The solution of a wave scattering problem to an ultra-short incident wave enables the derivation of these scattering parameters with only one time domain solution. The adaptive operations of a spacetime discontinuous Galerkin method and several or its unique properties, such as linear solution complexity and local / asynchronous solution features, enable accurate computation of scattering parameters. An inverse parameter retrieval method, from the equivalent material impedance and wave speed to dispersive elastic constitutive parameters, is uniquely solved by using the continuity of the wavenumber.

INTRODUCTION

For elastodynamics primary fields strain ε, stress σ, linear momentum $\mathbf{p}$, and velocity $\mathbf{v}$ are related by constitutive equations in the form $\varepsilon = \mathbf{D}\sigma$ and $\mathbf{p} = \rho\mathbf{v}$, where $\mathbf{D}$ is the compliance tensor and ρ is mass density. For one dimensional wave propagation only nonzero components of the fields are considered and the compliance matrix can be represented by a scalar D whose value can be determined from the dimension of problem and wave propagation mode (longitudinal versus shear). There are several approaches including field averaging and parameter retrieval methods to characterize dispersive, *i.e.,* frequency-dependent, constitutive parameters of an elastodynamic medium; *cf.* [1, 2] for a detailed review of dynamic homogenization. Figure 1 shows the concept of parameter retrieval method for a one dimensional wave through a slab l. By having the impedance $Z = \sqrt{\rho/D}$ and wave speed $c = 1/\sqrt{D\rho}$ of the slab and the constitutive parameters of the ambient D_0 and ρ_0 one can compute transmission and reflection of the slab for all frequencies.

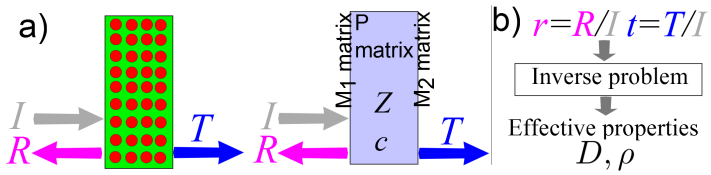

FIGURE 1. SCHEMATIC OF THE PARAMETER RETRIEVAL METHOD. FROM COMPUTATIONALLY OR EXPERIMENTALLY MEASURED REFLECTION AND TRANSMISSION COEFFICIENTS OF A SLAB OF COMPLEX MATERIAL, IMPEDANCE / WAVESPEED AND CONSEQUENTLY COMPLIANCE / MASS DENSITY OF AN EQUIVALENT MATERIAL ARE OBTAINED.

In the parameter retrieval method an inverse problem is solved; the transmission and reflection coefficients are obtained either experimentally or computationally for a slab of possibly complex structure and equivalent impedance Z and wave speed c are sought such that a slab of uniform Z and c yields the same scattering parameters. A schematic of the inverse problem is

*Address all correspondence to this author.

shown in Fig. 1b).

The retrieved parameters for Z and c (and consequently D and ρ) are functions of angular frequency ω. These functions can either be directly characterized by a frequency domain (FD) approach, where the retrieval method is solved for discrete set of frequencies of interest, or a time domain (TD) approach. In TD approaches the solution of scattering problem to a temporally short signal and a subsequent Fourier transform yield retrieved parameters for a wide range of frequencies. While FD approaches are more direct, each frequency requires a separate solution to an elliptic partial differential equation (PDE). As the problem complexity increases or higher or larger number of frequencies are considered, a TD approach can become more efficient as demonstrated in [3]. This is due to the fact that only one TD simulation is needed and TD hyperbolic PDE solvers can have a much better solution complexity versus the number of elements than elliptic PDE solvers. Please refer to [4] for a more thorough review of the advantages of TD approaches, in particular the spacetime discontinuous Galerkin (SDG) method, for the characterization of dispersive media.

In this manuscript an SDG method is presented that furthers the advantages of other existing TD approaches, *e.g.,* [3], in deriving scattering parameters by its various unique properties particularly mesh adaptivity in spacetime. Subsequently, an approach based on the continuity of wavenumber k is presented that can uniquely determine the values of D and ρ from Z and c.

Discontinuous Galerkin method

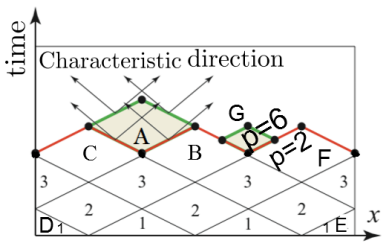

FIGURE 2. SPACETIME DISCRETIZATION USED IN THE SDG METHOD.

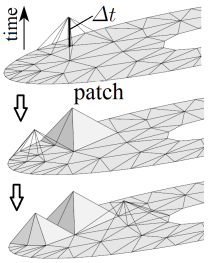

FIGURE 3. PATCH-BY-PATCH SOLUTION PROCEDURE.

The *spacetime discontinuous Galerkin* (SDG) method is a discontinuous Galerkin (DG) method that directly discretizes the spacetime using unstructured grids. The formulation of the SDG method for elastodynamics problem is presented in [5], but for completeness a brief review of the method is repeated here from prior publications. Many exceptional properties of the method stem from the use of *causal* meshes. For example in Fig. 2 the solution of element A depends only on the solution of earlier elements B and C given that the red facets are causal (fastest waves shown in arrows only pass in one direction through the facet). The level-1 elements depend only on initial conditions and boundary conditions for the elements D and E. The level-1 element solutions can be computed locally. Thus, causal SDG meshes enable asynchronous, element-by-element solutions with linear solution complexity. For more information the readers are referred to [5].

The individual elements in the $1d\times$time are replaced with small clusters of simplicial elements called *patches*, where only the exterior patch facets need to be causal as shown in Fig. 3 for clusters of tetrahedral elements in $2d\times$time. Using an advancing-front procedure, in each step the *Tent Pitcher* algorithm [6] advances in time a vertex in the *front mesh* to define a local front update; the causality constraint limits the maximum time increment Δt at the vertex. New patches are solved as local problems and update the current front, until the entire spacetime analysis domain is solved.

An h-adaptive formulation and implementation of the SDG method is presented in [7]. Some unique consequences of using unstructured and causal grids in spacetime are: 1) As other DG methods element interpolation order or size can suddenly change from one elements to its neighboring elements without the need for any transition elements as in conventional finite element methods; 2) Due to the causality of the grid and patch-by-patch solution procedure, adaptivity decisions are local. In contrast, implicit time marching schemes require a global resolution of a time step if a few elements are rejected; 3) If the spatial size of an element decreases, its temporal size is automatically decreased by causality of the element; *cf.* element G in Fig. 3. Simultaneous mesh adaptation in space and time is an immensely important aspect for having a fully efficient adaptive scheme in dynamics. In time marching explicit methods spatially small elements that are potentially generated by adaptive operations can significantly restrict time advance limit for the entire domain. This makes it difficult to achieve high refinement ratios (ratio of domain to the smallest element size) in practice, whereas refinement ratios of order 10^4 or larger are regularly experienced with the SDG method; *cf.* [7]; 4) Arbitrary high temporal orders of accuracy can be achieved at individual element level. In contrast, conventional time marching schemes often suffer from low temporal order of accuracy and the geometric stiffness problem discussed under item 3. The advantages of the SDG method are further clarified in the numerical results section.

FORMULATION

TD wave scattering analysis

Figure 4 shows a schematic of the problem set-up to determine scattering parameters of a unit cell by a TD analysis. A planar wave $I(t)$ impinges on the unit cell from the left side. The wave is reflected to the left, dissipated in the unit cell (if any of

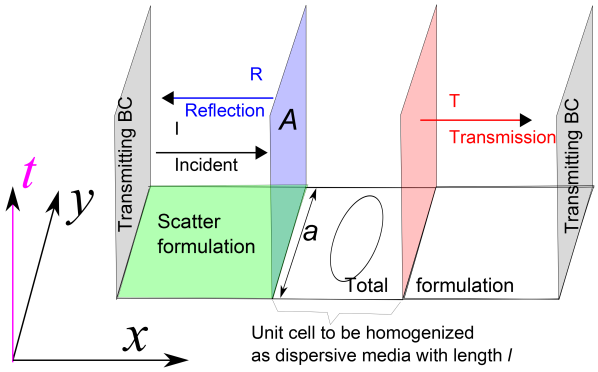

FIGURE 4. DERIVATION OF SCATTERING PARAMETERS FROM A TIME DOMAIN (TD) ANALYSIS. THE FOURIER TRANSFORMS OF REFLECTED (R) AND TRANSMITTED (T) WAVES IN RESPONSE TO A TEMPORALLY SHORT INCIDENT PULSE (I), YIELD TRANSMISSION AND REFLECTION COEFFICIENTS FOR A WIDE RANGE OF FREQUENCIES.

its constituents are not fully elastic), and transmitted to the domain on the right. The temporal function $I(t)$ should have a rich FD representation to enable parameter retrieval for a wide range or frequencies. It also has to be extremely close to zero at initial time $t = 0$ and final time $t = \bar{T}$ so that the problem can start by zero initial condition and be terminated at the final time without having any significant, *i.e.,* nonzero, solution fields beyond $t = \bar{T}$. In addition, they enable accurate representation of Fourier transform by $\overline{f}(\omega) = \int_{-\infty}^{\infty} f(t)e^{-j\omega t}\,\mathrm{d}t \approx \int_0^{\bar{T}} f(t)e^{-j\omega t}\,\mathrm{d}t$. A common choice for the incident wave is a Gaussian pulse,

$$I(t) = \sin(\omega_0 t)e^{-(t-t_0)^2/\varsigma^2} \tag{1}$$

with the Fourier transform,

$$\bar{I}(\omega) = \frac{1}{2} j\varsigma \exp(-j\omega t_0)\left[e^{-\frac{\varsigma^2}{2}(\omega+\omega_0)^2} - e^{-\frac{\varsigma^2}{2}(\omega-\omega_0)^2}\right] \tag{2}$$

where t_0 and ς are two time scales and ω_0 is a reference frequency. It is evident from Eqn. (2) that $\bar{I}$ has its most dominant frequency content in $[\omega_{\min}, \omega_{\max}] = [\omega_0 - 1/\varsigma, \omega_0 + 1/\varsigma]$. Thus, if the minimum and maximum frequencies desired for the characterization of unit cell are known ς and ω_0 are computed by $\omega_0 = 0.5(\omega_{\max} + \omega_{\min})$ and $\varsigma = 2/(\omega_{\max} - \omega_{\min})$. The role of $t_0 > 0$ is to make $I(t)$ weak enough at initial time $t = 0$, so that the problem shown in Fig. 1 can be initialized by zero initial condition without inducing large errors. In practice, $t_0 \gtrapprox 3\varsigma$ is used. The final time $\bar{T}$ is chosen such that $I(t)$ and elastic waves in the unit cell have attenuated sufficiently.

In order to more easily measure the reflected waves on the left side of the unit cell and implement a transmitting boundary on its far left end, a total field / scatter field (TF/SF) formulation is employed; that is, a SF formulation is used on the left side and TF is used in the unit cell and its right side (where transmitting waves are measured). In the present work, a simple first order transmitting boundary condition is employed on the left and right far ends of the domain; *cf.* [5] for the Riemann solution for this boundary condition. The top and bottom boundaries of the domain in general use a periodic boundary condition, implied by the repetition of the unit cell. However, for the problems considered here the unit cell is symmetric in both directions and the simpler symmetric boundary condition can be used on the top and bottom boundaries. The symmetry in the other direction, *e.g.,* along an axis parallel to y axis, ensures that a simple constitutive equation of the form $\boldsymbol{\varepsilon} = \mathbf{D}\boldsymbol{\sigma}$ and $\mathbf{p} = \rho\mathbf{v}$ can be employed. Otherwise, the more general Willis-type constitutive equations [8, 9] should have been employed.

Transmission / reflection coefficients in FD

The reflection coefficient in FD is obtained by computing the spatial average of $\overline{R}(\omega, y) = \int_{-\infty}^{\infty} R(t,y)e^{-j\omega t}\mathrm{d}t$, where $R(t,y)$ is the reflected wave on the scatter side of interface $A = a \times [t_0, \bar{T}]$ in Fig. 4 and a is the spatial domain on the reflection boundary at $t = 0$. By integrating $\overline{R}(\omega, y)$ over y spatially-averaged reflection coefficient are obtained. Noting this and the fact that elastic fields are almost zero outside $t \in [t_0, \bar{T}]$, spatially averaged reflection coefficient becomes $\overline{R}(\omega) = \frac{1}{|a|}\int_A R(t,y)e^{-j\omega t}\mathrm{d}A$ where $|a|$ is the measure of a. This integration is carried over triangular faces of the SDG discretization that lie on A. The transmission coefficient in frequency domain is computed similarly on the the right side of the unit cell. The magnitude of incident I, reflected R, and transmitted T waves are all computed based on the nonzero component of the traction vector on the x-normal plane. This corresponds to σ_{xx} for longitudinal constitutive parameters considered in this manuscript. Finally, transmission and reflection coefficients are obtained by $\bar{r}(\omega) = \frac{\overline{R}(\omega)}{\overline{I}(\omega)}$ and $\bar{t}(\omega) = \frac{\overline{T}(\omega)}{\overline{I}(\omega)}$.

Derivation of constitutive parameters

For a slab with impedance Z and wave speed c in an ambient domain with compliance D_0 and mass density ρ_0, its transmission and reflection coefficients are obtained by using two matching matrices (M1, M2) at the interfaces and one propagation matrix (P) as shown in Fig. 1a) to obtain,[1]

$$r = I_r \frac{z^2 - 1}{z^2 - I_r^2}, \quad t = z.\frac{1 - I_r^2}{z^2 - I_r^2} \tag{3}$$

[1] Derivation of scattering coefficients for the similar electromagnetics problem can be found in [10], chapter 6.

where $I_r = (Z - Z_0)/(Z + Z_0)$ is the reflection coefficient at the left interface and $Z_0 = \sqrt{\rho_0/D_0}$ is the impedance of the ambient. The parameter z is $z = e^{jkl}$, where $k = \omega/c$ is the wavenumber of wave in the medium and l is its length; *cf.* Fig. 4. There are many studies on the inversion of Eqn. (3) to obtain Z and c once r and t are known, see for example [11–13]. Herein a process given by [14] is followed where Z and z are given by,

$$Z = Z_0\sqrt{\frac{(r+1)^2 - t^2}{(r-1)^2 - t^2}}, \quad z = \frac{(Z+Z_0) - r(Z-Z_0)}{t(Z+Z_0)} \tag{4}$$

The plus/minus choices of square root in the equation for Z result in z and $1/z$ values but as discussed in [14] both choices eventually result in the same effective material properties. However, there is an inherent ambiguity in deriving wavenumber k from z because of the phase ambiguity of log function; that is, by taking the log of $z = e^{jkl}$ we obtain,

$$k = \frac{\phi}{l} - j\frac{\log|z|}{l}, \quad \text{where} \quad \phi := \theta + 2p\pi \tag{5}$$

and $|z|$ and $\theta \in [0, 2\pi)$ are used in polar expression of $z = |z|e^{j\theta}$. That is, the phase angle of kl is obtained only within arbitrary number of full wave traveling in the slab. One approach to resolve this non-uniqueness in the inverse problem is to start from low frequencies where $p = 0$ and as ω increases determine the correct value of p by preserving the continuity of wavenumber. A similar approach is taken in [13,15] for electromagnetics problem. Finally, after k and Z are obtained, elastic constitutive equations are given by $D = \frac{k}{Z\omega}$ and $\rho = \frac{kZ}{\omega}$.

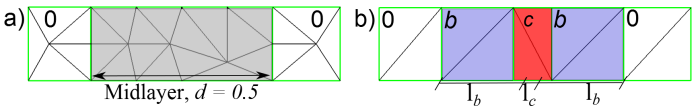

FIGURE 5. INITIAL MESHES FOR a) A FULLY ELASTIC MIDLAYER A, b) 3-LAYER SET BCB OF MATERIALS B AND C.

NUMERICAL RESULTS

Figure 5 shows the schematic of the unit cell and the initial meshes used for the two one-dimensional problems considered herein. For the first problem, a fully elastic single layer with compliance $D = 0.1$ and and density $\rho = 1$ is characterized. The values of $D_0 = 1$ and $\rho_0 = 1$ are chosen for the ambient medium. The goal of this example is to demonstrate that the parameter retrieval method recovers nondispersive elastic properties $D = 0.1$ and $\rho = 1$. Figure 6 compares computationally obtained real part of transmission coefficient with the exact value, with the former obtained by the Fourier transform of the SDG method's TD solution and the latter from matching / propagation matrix method. The retrieved values for D and ρ, shown in Fig. 7, are very close to the exact values almost everywhere; the regions with larger error correspond to regions where numerator and denominator terms in Eqn. (4) approach zero.

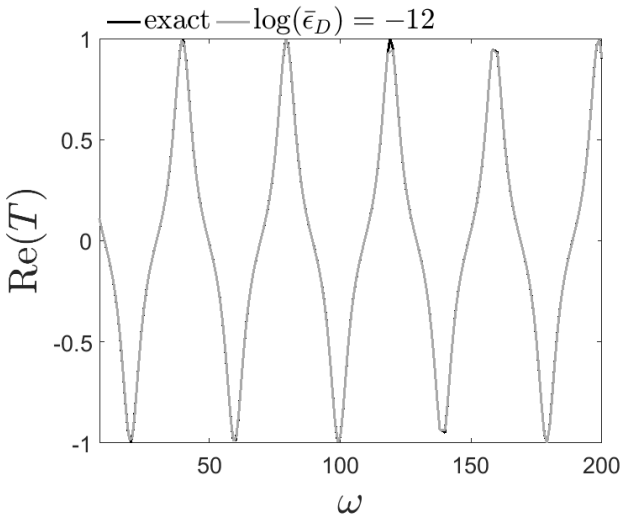

FIGURE 6. COMPARISON OF NUMERICAL AND ANALYTICAL REAL PART OF TRANSMISSION COEFFICIENT FOR A FULLY ELASTIC ONE LAYER UNIT CELL.

The second example is taken from [16], where material b and c have properties $C_b = 8.68$ GPa, $\rho_b = 1.18$ g/cm^3 and $C_c = 320$ GPa, $\rho_c = 7.954$ g/cm^3, respectively. The thicknesses are $l_b = 1.5$ mm and $l_c = 0.8$ mm. The ambient medium properties are stiffness $C_0 = 10$ GPa, and mass density $\rho_0 = 1$ g/cm^3. As mentioned before, one critical step in parameter retrieval method is the determination of p for computing the wavenumber k in Eqn. (5). Figure 8 depicts p and phase ϕ, divided by 2π, for the range of frequencies considered. As it can be seen for $\omega \in [1.24, 2.82]$Mrad/s the phase angle for kl is the constant value $\phi = \pi$. In fact, this region corresponds to a stopband because the imaginary part of k becomes nonzero. Past $\omega = 2.82$Mrad/s there is a shift in the value of p from 0 to 1. This ensures the continuity of wavenumber k. Once k and Z are determined, C and ρ are computed from $C = \frac{Z\omega}{k}$ and $\rho = \frac{kZ}{\omega}$. Figure 9 shows the retrieved value for C which is almost identical to the exact solution obtained by matching/propagation matrix approach.

The last problem considered corresponds to an elastodynamics metamaterial set-up from [17] where circular lead inclusions are surrounded by rubber layers and are repeated in an epoxy matrix. Figure 10 shows the initial mesh for this problem. A

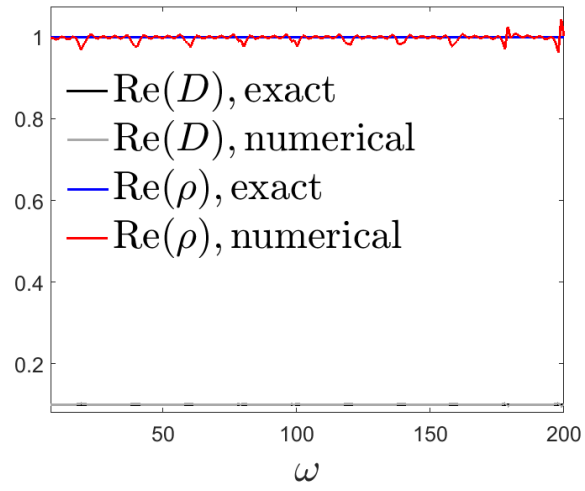

FIGURE 7. COMPARISON OF NUMERICALLY RETRIEVED AND EXACT COMPLIANCE D AND MASS DENSITY ρ FOR A FULLY ELASTIC ONE LAYER UNIT CELL. REGIONS OF LARGER ERROR CORRESPOND TO FREQUENCIES WHERE THE NUMERATOR OR DENOMINATOR OF Z IN EQUATION (4) TENDS TO ZERO.

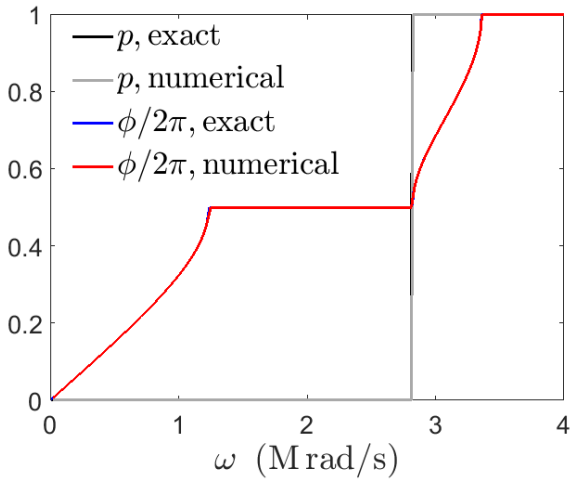

FIGURE 8. THE INTEGER p AND SCALED PHASE $\phi/2\pi$, FROM EQUATION (5), IN THE PARAMETER RETRIEVAL STAGE FOR 3-LAYER UNIT CELL, FOR THE ANALYTICAL AND NUMERICAL SOLUTIONS OBTAINED BY THE MATCHING / PROPAGATION MATRIX METHOD AND THE SDG METHOD, RESPECTIVELY. THE REGIONS WITH CONSTANT $\phi = \pi$ AND $\phi = 2\pi$ CORRESPOND TO THE FIRST AND SECOND STOPBANDS.

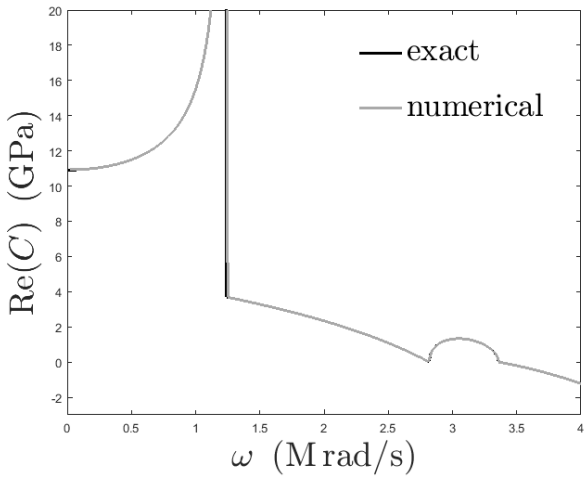

FIGURE 9. THE COMARISON OF NUMERICAL AND ANALYTICAL REAL PART OF COMPLIANCE C FOR THE 3-LAYER UNIT CELL.

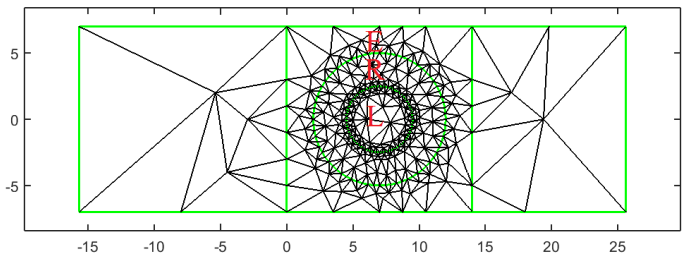

FIGURE 10. INITIAL MESH FOR THE CIRCULAR INCLUSION UNIT CELL AND REFLECTION / REFLECTION SIDES.

sequence of solution visualization is shown in Fig. 11, where internal and kinetic energy densities are mapped to color and height fields, respectively. One interesting observation is very large oscillations of the heavy lead sphere in its very compliant rubber surrounding, as evident in Figs. 11b) to 11d). Also, it appears that a considerable amount of energy remains in the unit cell by local scattering of waves in the rubber layer. In fact, the final time used for this simulation is much larger than $\varsigma = 1\ \mu$s ($\bar{T} \approx 140\varsigma$) to ensure attenuation of elastic fields in the unit cell. A small damping coefficient is used in the rubber layer. To demonstrate the advantage of using the SDG method for this problem, the temporal intersection of spacetime mesh at time $t = 32\ \mu$s is shown Fig. 12. Spacetime adaptive operations have created very small elements in regions with high gradient solutions, while the trailing regions of moving fronts are coarsened. The transmission coefficients for this problem are shown in Fig. 13.

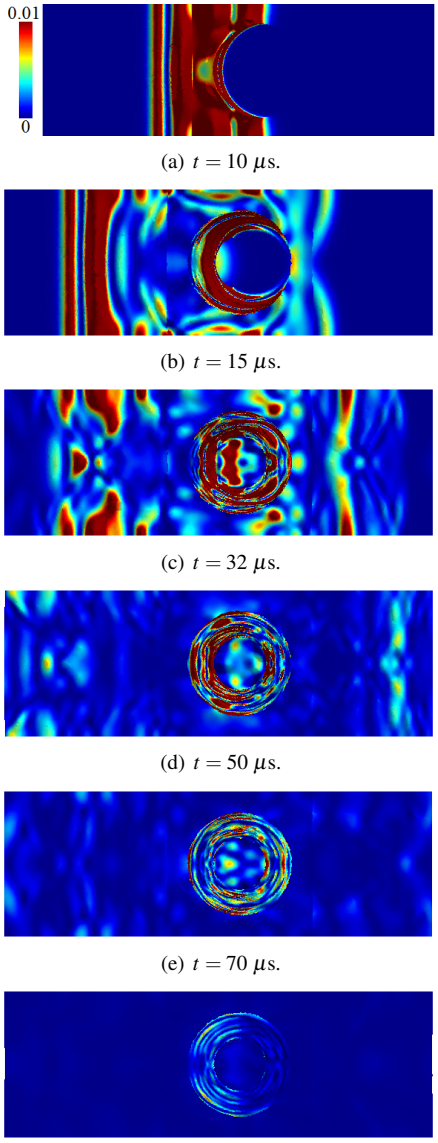

(a) $t = 10\ \mu$s.

(b) $t = 15\ \mu$s.

(c) $t = 32\ \mu$s.

(d) $t = 50\ \mu$s.

(e) $t = 70\ \mu$s.

(f) $t = 130\ \mu$s.

FIGURE 11. TIME SEQUENCE OF WAVE PROPAGATION IN CIRCULAR INCLUSION UNIT CELL. STRAIN AND KINETIC ENERGY DENSITIES ARE MAPPED TO COLOR AND HEIGHT FIELDS, RESPECTIVELY.

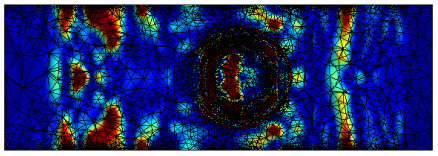

FIGURE 12. SUPERPOSITION OF SPACETIME MESH INTERSECTION AND SDG SOLUTION AT TIME $t = 32\ \mu$s.

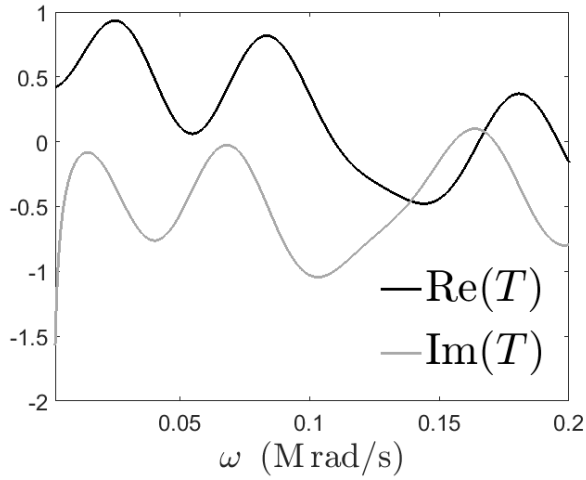

FIGURE 13. THE REAL AND IMAGINERY PARTS OF TRANSMISSION COEFFICIENT FOR THE CIRCULAR INCLUSION UNIT CELL PROBLEM.

CONCLUSIONS

An efficient TD approach was presented to computationally derive transmission and reflection coefficients of an elastodynamic unit cell. The solution to only one TD solution to a problem with a ultra-short temporal pulse and employing the SDG methods highly advanced adaptive operations in spacetime enabled very accurate computation of these scattering parameters. The continuity of wavenumber was used as a means to eliminate non-uniqueness in the elastic parameter retrieval from scattering parameters.

REFERENCES

[1] Charalambakis, N., 2010. "Homogenization techniques and micromechanics. a survey and perspectives". *Applied Mechanics Reviews,* ***63***(3), pp. 1–10.

[2] Srivastava, A., 2015. "Elastic metamaterials and dynamic homogenization: A review". *International Journal of Smart and Nano Materials,* ***6***(1), pp. 41–60.

[3] Busch, K., Konig, M., and Niegemann, J., 2011. "Discontinuous Galerkin methods in nanophotonics". *Laser Photonics Reviews,* ***5***(6), pp. 773–809.

[4] Abedi, R., Omidi, O., and Clarke, P., 2014. "Spacetime discontinuous Galerkin FEM: Spectral response". In Journal of Physics: Conference Series, XXII International Conference on Spectral Line Shapes 2014: IOP Publishing, p. 012065.

[5] Abedi, R., Haber, R. B., and Petracovici, B., 2006. "A spacetime discontinuous Galerkin method for elastodynamics with element-level balance of linear momentum". *Com-*

puter Methods in Applied Mechanics and Engineering, ***195***, pp. 3247–3273.

[6] Abedi, R., Chung, S.-H., Erickson, J., Fan, Y., Garland, M., Guoy, D., Haber, R., Sullivan, J. M., Thite, S., and Zhou, Y., 2004. "Spacetime meshing with adaptive refinement and coarsening". In Proceedings of the Twentieth Annual Symposium on Computational Geometry, SCG '04, ACM, pp. 300–309.

[7] Abedi, R., Haber, R. B., Thite, S., and Erickson, J., 2006. "An *h*–adaptive spacetime–discontinuous Galerkin method for linearized elastodynamics". *Revue Européenne de Mécanique Numérique (European Journal of Computational Mechanics),* ***15***(6), pp. 619–642.

[8] Milton, G. W., and Willis, J. R., 2007. "On modifications of newton's second law and linear continuum elastodynamics". In Proceedings of the Royal Society of London A: Mathematical, Physical and Engineering Sciences, Vol. 463, The Royal Society, pp. 855–80.

[9] Willis, J., 2012/04/. "The construction of effective relations for waves in a composite". *Comptes Rendus Mecanique,* ***340***(4-5), pp. 181–92.

[10] Orfanidis, S. J., 2014. *Electromagnetic waves and antennas*.

[11] Smith, D., Schultz, S., Markoš, P., and Soukoulis, C., 2002. "Determination of effective permittivity and permeability of metamaterials from reflection and transmission coefficients". *Physical Review B,* ***65***(19), p. 195104.

[12] Fokin, V., Ambati, M., Sun, C., and Zhang, X., 2007. "Method for retrieving effective properties of locally resonant acoustic metamaterials". *Physical Review B (Condensed Matter and Materials Physics),* ***76***(14), pp. 144302 – 1.

[13] Shi, Y., Li, Z.-Y., Li, L., and Liang, C.-H., 2016. "An electromagnetic parameters extraction method for metamaterials based on phase unwrapping technique". *Waves in Random and Complex Media,* ***26***(4), pp. 417–33.

[14] Arslanagić, S., Hansen, T. V., Mortensen, N. A., Gregersen, A. H., Sigmund, O., Ziolkowski, R. W., and Breinbjerg, O., 2013. "A review of the scattering-parameter extraction method with clarification of ambiguity issues in relation to metamaterial homogenization". *IEEE Antennas and Propagation Magazine,* ***55***(2), pp. 91–106.

[15] Abedi, R., and Mudaliar, S., August 19-26, 2017. "A spacetime adaptive approach to characterize complex dispersive media". In In Proceedings of 32nd International Union of Radio Science General Assembly & Scientific Symposium (URSI GASS).

[16] Nemat-Nasser, S., Willis, J. R., Srivastava, A., and Amirkhizi, A. V., 2011. "Homogenization of periodic elastic composites and locally resonant sonic materials". *Physical Review B,* ***83***(10), p. 104103.

[17] Liu, Z., Chan, C., and Sheng, P., 2005. "Analytic model of phononic crystals with local resonances". *Physical Review B,* ***71***(1), p. 014103.